Cytotoxic and Antiangiogenetic Xanthones Inhibiting Tumor Proliferation and Metastasis from *Garcinia xipshuanbannaensis*

Xuke Zhang,[†,¶] Ziteng Song,[†,¶] Ying Li,[†] Huimei Wang,[†] Shaojie Zhang,[†] Anna-Mari Reid,[‡] Namrita Lall,[‡] Jie Zhang,[§] Chunyan Wang,[⊥] Dongho Lee,[#] Yasushi Ohizumi,[∇] Jing Xu,*[,†] and Yuanqiang Guo*[,†]

[†]State Key Laboratory of Medicinal Chemical Biology, College of Pharmacy, and Tianjin Key Laboratory of Molecular Drug Research, Nankai University, Tianjin 300350, People's Republic of China

[‡]Department of Plant and Soil Sciences, University of Pretoria, Pretoria 0002, South Africa

[§]Key Laboratory for Green Processing of Chemical Engineering of Xinjiang Bingtuan, School of Chemistry and Chemical Engineering, Shihezi University, Shihezi 832003, People's Republic of China

[⊥]Tianjin Second People's Hospital, Tianjin 300192, People's Republic of China

[#]College of Life Sciences and Biotechnology, Korea University, Seoul 02841, Republic of Korea

[∇]Kansei Fukushi Research Institute, Tohoku Fukushi University, 6-149-1 Kunimigaoka, Aoba-ku, Sendai 989-3201, Japan

ABSTRACT: Eight prenylated xanthones including four new analogues were extracted and purified from the leaves of *Garcinia xipshuanbannaensis*. Multiple techniques including UV, 1D and 2D NMR, and HRESIMS were used to determine the structures of the isolated xanthones. Theses xanthones were evaluated for their cytotoxicity toward human cancer cells, and compound **4** exhibited activity against HeLa cells. A cytotoxic mechanism examination revealed the active compound induced cell apoptosis by arresting cell cycle, increasing the levels of ROS, and inhibiting the expression of p-STAT3 in HeLa cells. In in vivo zebrafish experiments, compound **4** was found to block tumor proliferation and migration and have antiangiogenetic activity, and seems worthy of further laboratory evaluation.

The genus *Garcinia* L., is the most predominant of the family Clusiaceae, and comprises approximately 450 species.[1,2] *Garcinia* species are distributed primarily in tropical Asia, southern Africa, and western Polynesia. Several *Garcinia* plants, such as *G. cowa*, *G. mangostana*, and *G. bracteata*, have been used as traditional or folk medicines for various medical indications.[1,2] Such medicinal applications are supported by the occurrence of chemical constituents present in these plants inclusive mainly of a variety of xanthones, flavonoids, and benzophenones, according to the previous literature.[1-19] Many members of these compound classes have exhibited a wide range of biological effects,[1,2,20-24] including cytotoxic, antimicrobial, antifungal, antioxidant, and antimalarial activities. The interesting polyprenylated structures and varied biological bioactivities of xanthones previously obtained drew our attention to *Garcinia* plants.

Garcinia xipshuanbannaensis Y. H. Li, a rare and endemic species, is indigenous to the south of Yunnan Province of the People's Republic of China.[25] Several xanthones, benzophenones, and flavonoids have been reported in *G. xipshuanbannaensis*, and some of these were reported to have cytotoxic activities.[26-28] Although many natural xanthones have been discovered from *Garcinia* plants and showed cytotoxic or antiproliferative activity, almost all of the biological studies conducted have been limited to preliminary investigations at the cellular level and only a few studies on in vivo antitumor effects have been performed. Considering the limited phytochemical information on *G. xipshuanbannaensis* and the general lack of in vivo antitumor studies on the xanthones, such an investigation on the chemical constituents of *G. xipshuanbannaensis* was conducted. During the phytochemical analysis conducted in the present study, four new prenylated xanthones, xipsxanthones A–D (**1**–**4**), along with four known analogues, were isolated and identified from the methanol extract of the leaves of *G. xipshuanbannaensis*. Herein, details of the isolation, structural determination, cytotoxic effects, preliminary action mechanism, and in vivo antitumor and antiangiogenetic effects using zebrafish models of these xanthones are reported.

■ RESULTS AND DISCUSSION

The methanol extract prepared from *G. xipshuanbannaensis* was fractionated by column

chromatographic techniques and purified further by HPLC to afford eight pure xanthones, for which the structures were elucidated as follows by UV, NMR, and HRESIMS data.

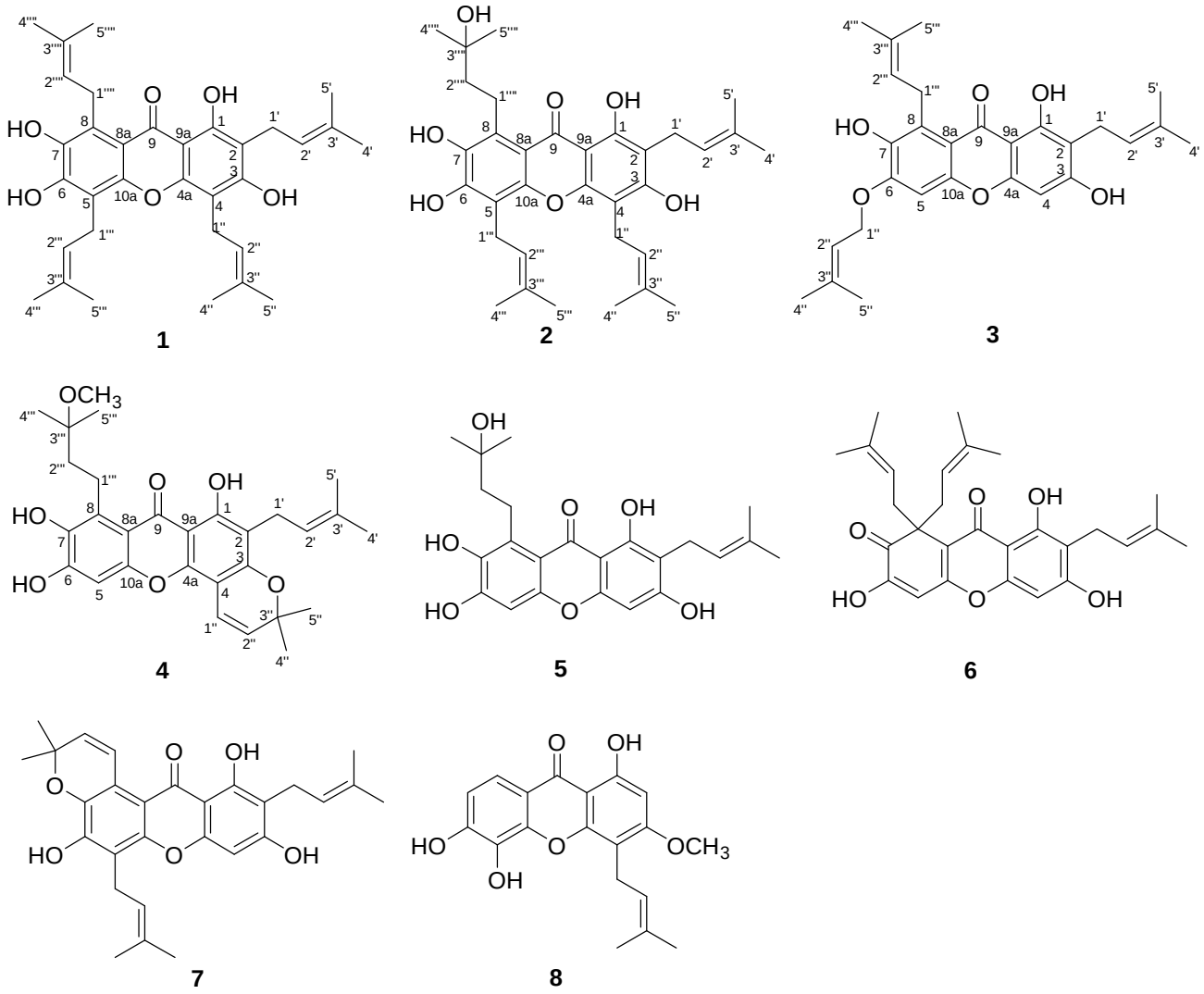

Compound **1** was isolated as a yellow powder. The molecular formula of $C_{33}H_{40}O_6$ was determined by a combination of its ^{13}C NMR and DEPT and HRESIMS data at *m/z* 531.2753 $[M - H]^-$ (calcd for $C_{33}H_{39}O_6$, 531.2747), consistent with 14 degrees of unsaturation. The UV spectrum showed characteristic xanthone absorption bands at 207, 247, 264, and 323 nm.[29,30] In accordance with the UV spectrum, a typical carbonyl carbon at δ_C 183.4 (C-9) and 12 aromatic signals (δ_C 158.4, 108.6, 159.8, 104.2, 152.1, 113.3, 148.6, 139.3, 124.6, 111.1, 103.5, 151.3) were observed in the ^{13}C NMR spectrum. These spectroscopic features implied compound **1** to have a xanthone skeleton.[31-35] Apart from the characteristic signals for the xanthone scaffold, the presence of four prenyl groups (3-methyl-2-butenyl group) were deduced from the olefinic carbons (δ_C 121.2, 121.9 × 2, 122.2, 134.9, 134.0 ×2, 135.1),

the aliphatic carbon signals (methylene signals at δ_C 21.6, 21.9, 22.7, and 25.8; methyl signals at δ_C 25.9 × 2, 25.8 × 2, 18.1, and 17.9 × 3), along with the typical olefinic methyl singlets (δ_H 1.88, 1.84, 1.82 × 2, 1.76 × 2, and 1.71×2) observed in the ^{1}H NMR spectrum. These inferences of the xanthone scaffold and four prenyl groups were confirmed by 1D and 2D NMR data analysis.

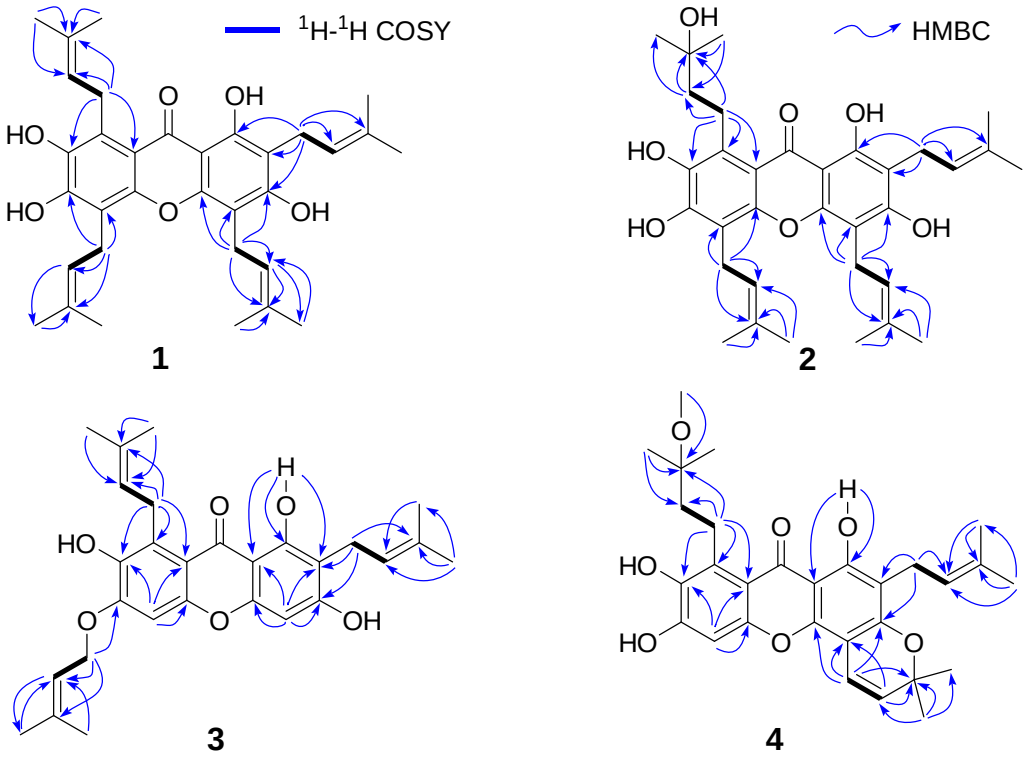

Figure 1. ^{1}H–^{1}H COSY and key HMBC correlations of compounds **1**–**4**.

The substituent pattern of **1** was determined by HMBC correlations (Figure 1) including those between a chelated hydroxy group at δ_H 13.74 (OH-1) to C-1 (δ_C 158.4), C-2 (δ_C 108.6), and C-9a (103.5), which indicated a hydroxy group was located at C-1. A long-range correlation of H_2-1' of the prenyl group at δ_H 3.45 to C-1 (δ_C 158.4), C-2 (δ_C 108.6), and C-3 (δ_C 159.8) was indicative of one prenyl group being attached at C-2. Similarly, the other three prenyl groups were found to be linked at C-4, C-5, and C-8 by the HMBC correlations of H_2-1" (δ_H 3.53) to C-3 (δ_C 159.8), C-4 (δ_C 104.2), and C-4a (δ_C 152.1), H_2-1'" (δ_H 3.62) to C-5 (δ_C 113.3), C-6 (δ_C 148.6), and C-10a (δ_C 151.3), and H_2-1"" (δ_H 4.30) to C-7 (δ_C 139.3), C-8 (δ_C 124.6), and C-8a (δ_C 111.1), respectively (Figure 1). No aromatic protons were observed in the ^{1}H NMR spectrum and three additional hydroxy groups were therefore assigned to C-3, C-6, and C-7 by additional analysis of the 1D and 2D NMR spectra, which was supported by the HRESIMS data. The 2D structure of **1** was thus established and the assignments of

the proton and carbon signals were accomplished by the full interpretation of NMR data. According to the above data analysis, compound **1** (xipsxanthone A) was elucidated as depicted.

Table 1. **^{13}C NMR Data for Compounds 1–4** ($CDCl_3$, 100 MHz, δ in ppm)

position	**1**		**2**		**3**		**4**	
1	158.4	C	158.4	C	160.5	C	155.9	C
2	108.6	C	108.5	C	108.3	C	106.4	C
3	159.8	C	159.6	C	161.3	C	157.0	C
4	104.2	C	104.2	C	93.0	CH	104.0	C
4a	152.1	C	152.1	C	155.0	C	153.7	C
5	113.3	C	113.0	C	97.7	CH	100.6	CH
6	148.6	C	151.5	C	150.9	C	153.5	C
7	139.3	C	138.5	C	140.4	C	139.2	C
8	124.6	C	127.3	C	126.9	C	129.7	C
8a	111.1	C	110.9	C	111.9	C	111.2	C
9	183.4	C	183.0	C	182.4	C	182.7	C
9a	103.5	C	103.5	C	103.8	C	103.6	C
10a	151.3	C	149.9	C	152.7	C	152.0	C
1'	21.6	CH_2	21.9	CH_2	21.4	CH_2	21.3	CH_2
2'	121.9	CH	122.2	CH	121.7	CH	122.4	CH
3'	134.9	C	134.7	C	135.4	C	131.2	C
4'	25.9	CH_3	25.9	CH_3	25.9	CH_3	25.8	CH_3
5'	18.1	CH_3	17.9	CH_3	18.1	CH_3	18.0	CH_3
1"	21.9	CH_2	21.2	CH_2	66.0	CH_2	116.2	CH
2"	121.9	CH	121.7	CH	118.0	CH	126.8	CH
3"	134.0	C	132.8	C	140.2	C	77.6	C
4"	25.9	CH_3	25.8	CH_3	25.9	CH_3	28.2	CH_3
5"	17.9	CH_3	17.9	CH_3	18.3	CH_3	28.2	CH_3
1"'	22.7	CH_2	21.6	CH_2	25.7	CH_2	20.9	CH_2
2"'	121.2	CH	122.0	CH	122.7	CH	41.8	CH
3"'	134.0	C	134.0	C	132.3	C	76.8	C
4"'	25.8	CH_3	25.8	CH_3	26.0	CH_3	24.2	CH_3
5"'	17.9	CH_3	17.9	CH_3	17.9	CH_3	24.2	CH_3
1""	25.8	CH_2	22.6	CH_2				
2""	122.2	CH	42.4	CH				
3""	135.1	C	73.0	C				
4""	25.8	CH_3	29.8	CH_3				
5""	17.9	CH_3	29.7	CH_3				
OCH_3							49.6	CH_3

Table 2. **^{1}H NMR Data for Compounds 1–4** ($CDCl_3$, 400 MHz, δ in ppm, J in Hz)

position	**1**	**2**	**3**	**4**
4			6.24 s	
5			6.66 s	6.83 s
1'	3.45 d (6.8)	3.44 d (6.7)	3.43 d (7.0)	3.42 d (7.2)
2'	5.27 m[a]	5.27 m[a]	5.29 m[a]	5.22 t (7.2)
4'	1.76 s	1.68 s	1.77 s	1.67 s
5'	1.88 s	1.83 s	1.84 s	1.87 s
1''	3.53 d (6.5)	3.54 d (7.0)	4.63 d (6.7)	6.75 d (10.0)
2''	5.27 m[a]	5.27 m[a]	5.49 t (6.7)	5.57 d (10.0)
4''	1.76 s	1.75 s	1.82 s	1.46 s
5''	1.82 s	1.83 s	1.77 s	1.46 s
1'''	3.62 d (6.9)	3.60 d (6.9)	4.11 d (6.7)	3.37 t (6.1)
2'''	5.27 m[a]	5.27 m[a]	5.31 m[a]	2.01 t (6.1)
4'''	1.71 s	1.74 s	1.69 s	1.23 s
5'''	1.84 s	1.81 s	1.85 s	1.23 s
1''''	4.30 d (6.3)	3.38 t (6.1)		
2''''	5.27 m[a]	1.98 t (6.1)		
4''''	1.71 s	1.32 s		
5''''	1.82 s	1.32 s		
OH-1	13.74 s	13.88 s	13.93 s	13.75 s
OCH_3				3.31 s

[a]Signals were in overlapped regions of the spectra and the multiplicities could not be discerned.

Compound **2** (xipsxanthone B) was obtained as a yellow gum. The molecular formula of $C_{33}H_{42}O_7$ was established by a combination of its 1D NMR and HRESIMS data at *m/z* 549.2855 $[M - H]^-$ (calcd for $C_{33}H_{41}O_7$, 549.2852). The same xanthone skeleton as that of **1** was revealed from the 12 aromatic carbons (δ_C 158.4, 108.5, 159.6, 104.2, 152.1, 113.0, 151.5, 138.5, 127.3, 110.9, 103.5, and 149.9) and a characteristic carbonyl carbon (δ_C 183.0). In addition to these carbons for the skeleton, the ^{13}C NMR spectrum exhibited additional 20 carbon signals, which comprised six olefinic carbons (δ_C 112.0, 121.7, 122.2, 132.8, 134.0, and 134.7), an oxygenated carbon (δ_C 73.0), and 13 aliphatic carbons (five methylenes and eight methyls) (Table 1). According to the characteristic signals for the prenyl groups as shown in compound **1**, three prenyl groups were deduced readily from the carbon and proton signals assignable to the three sets of prenyl moieties (Table 2). Apart from these carbons, five carbon resonances remained including one oxygenated carbon (δ_C 73.0), two methylenes (δ_C 22.6 and 42.4), and two methyls (δ_C 29.8 and 29.7). These five carbons, together with the corresponding methyl and

methylene protons (Table 2), constituted a 3-hydroxy-3-methylbutyl group, which was concluded from the analysis of HMQC and HMBC spectra. The HMBC correlations of H_2-1' to C-1, C-2, and C-3, were supportive of one prenyl group assignable to C-2. Similarly, two additional prenyl groups located at C-4 and C-5 were inferred from the long-range couplings of H_2-1" to C-3, C-4, and C-4a, H_2-1"' to C-5, C-6, and C-10a. The remaining 3-hydroxy-3-methylbutyl group was found to be located at C-8 from the HMBC correlation of H_2-1"" to C-7, C-8, and C-8a. No other carbon resonances were found in the ^{13}C NMR spectrum, so four hydroxy groups were assigned to C-1, C-3, C-6, and C-7, as supported by the HRESIMS data. All of the above data were supportive of the assignment of the structure for compound **2** as shown.

Compound **3** was obtained as a yellow gum and gave a molecular formula of $C_{28}H_{32}O_6$, based on the HRESIMS peak at *m*/*z* 463.2122 $[M - H]^-$ (calcd for $C_{28}H_{31}O_6$, 463.2122) and the ^{13}C NMR data. The ^{1}H NMR spectrum showed two aromatic proton signals [(δ_H 6.24, 1H, s) and (δ_H 6.66, 1H, s)]. In the ^{13}C NMR spectrum, 12 aromatic carbons and one carbonyl carbon (Table 1) were supportive of the occurrence of the same xanthone scaffold as those of compounds **1** and **2**. In addition to the skeletal carbon signals, there were 15 extra resonances, which were inferred to form three sets of prenyl groups consistent with polyprenyl-substituted xanthones reported in the literature.[31-35] The residual five carbons [two olefinic (δ_C 118.0 and 140.2), one oxygenated (δ_C 66.0), and two methyls (δ_C 25.9 and 18.3)], as well as the typical proton signals (Table 2) were indicative of a 1-hydroxy-3-methyl-2-butenyl group, namely, an *O*-prenyl group, which was verified by analysis of the 1D and 2D NMR data.[36,37] The HMBC correlations (Figure 1) from H_2-1' to C-1–C-3, H_2-1" to C-6, and H_2-1"' to C-7, C-8, and C-8a, indicated the *O*-prenyl and two prenyl groups to be attached to C-6, C-2, and C-8, respectively. The HRESIMS data also supported the presence of three hydroxy groups, which were assigned to C-1, C-3, and C-7 from the NMR data analysis. The structure of compound **3** (xipsxanthone C) was assigned accordingly, as shown.

Compound **4** was obtained as a yellow solid and gave a molecular formula $C_{29}H_{34}O_7$ on the grounds of the HRESIMS ion peak at *m*/*z* 495.2384 $[M + H]^+$ (calcd for $C_{29}H_{35}O_7$, 495.2383), which was

supported by the corresponding 1D NMR data. From the ^{1}H and ^{13}C NMR spectra, one prenyl group and the same xanthone framework as present in compounds **1**–**3** were inferred from the typical carbonyl, aromatic, and olefinic carbons (Tables 1 and 2). In addition to these carbons for the skeleton and the prenyl moiety, the ^{13}C NMR spectrum exhibited additional 11 carbon signals, which comprised two olefinic carbons (δ_C 116.2 and 126.8), three oxygenated carbons (δ_C 77.6, 76.8, and 49.6), and six aliphatic carbons [two methylenes (δ_C 20.9 and 41.8) and four methyls (δ_C 28.2 × 2 and 24.2 ×2)] (Table 1). Through analysis of the HMQC and HMBC spectra, the 11 carbons were found to constitute two substituent groups derived from prenyl groups including a 3-hydroxy-3-methylbutenyl group and a 3-methoxy-3-methylbutyl group, of which the former formed a pyran ring composed of C-3, C-4, C-1", C-2", and C-3", as inferred from the 1D and 2D NMR data. HMBC correlations were used to reveal the locations of the remaining two substituent groups. From the HMBC correlations of H_2-1' to C-1, C-2, and C-3, the prenyl group was assigned to C-2. Similarly, the 3-methoxy-3-methylbutyl group at C-8 was deduced from the long-range couplings of H-1'" to C-7, C-8, and C-8a. No other carbon resonances remained in the ^{13}C NMR spectrum, so three hydroxy groups were assigned to C-1, C-6, and C-7, as supported by the HRESIMS data. Thus, compound **4** (xipsxanthone D) was established as depicted.

Four known compounds were isolated and identified in the present study as garcinone C (5),[38] allanxanthone C (6),[39] tovophyllin A (7),[40,41] and dulxanthone A (8),[42] respectively, by comparison of their physical and spectroscopic data obtained with those reported previously. Compound **8** was isolated from this plant for the first time.

According to the literature,[1,2,43-46] cytotoxicity is one of the most frequently reported biological effects of xanthones, with cancer being a severe and enormous threat to human health. Thus, these isolates were subjected to cytotoxic evaluation using an MTT assay. Homoharringtonine was used as the positive control.[47] The results showed that compound **4** had an inhibitory activity with an IC_{50} value of 9.6 μM against HeLa cells (IC_{50} value of homoharringtonine, 0.4 μM), while it was inactive (IC_{50} > 10 μM) against K562 and HepG2 cells, all other compounds tested were inactive for all cell lines used.

To investigate the possible cytotoxic mechanism induced by compound **4**, an annexin V/PI double staining assay was performed,[47,48] which indicated the apoptotic effects on HeLa cells. As displayed in Figure 2, the annexin V/PI staining assay showed that the population of PI positive cells increased dramatically. With the increase of concentrations of compound **4**, the percentage of apoptotic cells rose from 14.59% (control) to 23.95% (6 μM), 26.49% (12 μM) and 33.70% (50 μM). The data indicated that the apoptosis of HeLa cells induced by compound **4** was dose-dependent.

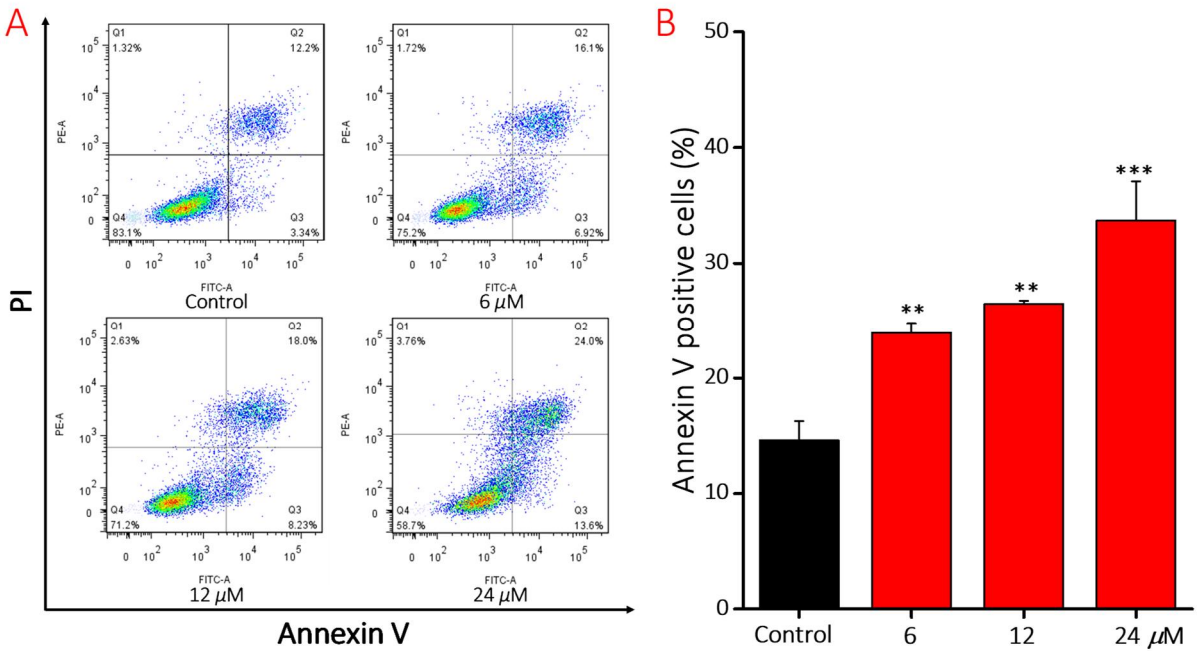

Figure 2. Apoptosis effects of HeLa cells induced by compound **4**. HeLa cells were treated with different concentrations (6, 12, and 24 μM) of compound **4** for 48 h. Then the cells were harvested, stained with Annexin V and propidium iodide (PI), and subsequently analyzed by flow cytometry. (Left) Flow cytometric analysis of HeLa cells after treated with different concentrations of compound 4. (Right) Histogram of apoptotic cells at 48 h with the treatment of compound **4**. Data from three separate experiments are expressed as means ± SD. (**) $p < 0.01$ and (***) $p < 0.001$ versus control group.

Apoptosis or programmed cell death is closely coupled with cell cycle progression. To examine the cause of HeLa cells apoptosis, the effects of compound **4** on cell cycle were further evaluated by flow cytometric analysis,[47,48] and the results were shown in Figure 3. With an increase in concentrations of compound **4** from 6 μM to 24 μM, the percentage of cells in the G0/G1 phase increased from 40.03% (control) to 55.33% (6 μM), 65.78% (12 μM), and 67.20% (24 μM), while the percentage of cells in the S- and G2 phases decreased after treatment at the different concentrations. These data revealed that compound **4** suppressed the G0/G1 transition of the cell cycle, leading to HeLa cell apoptosis.

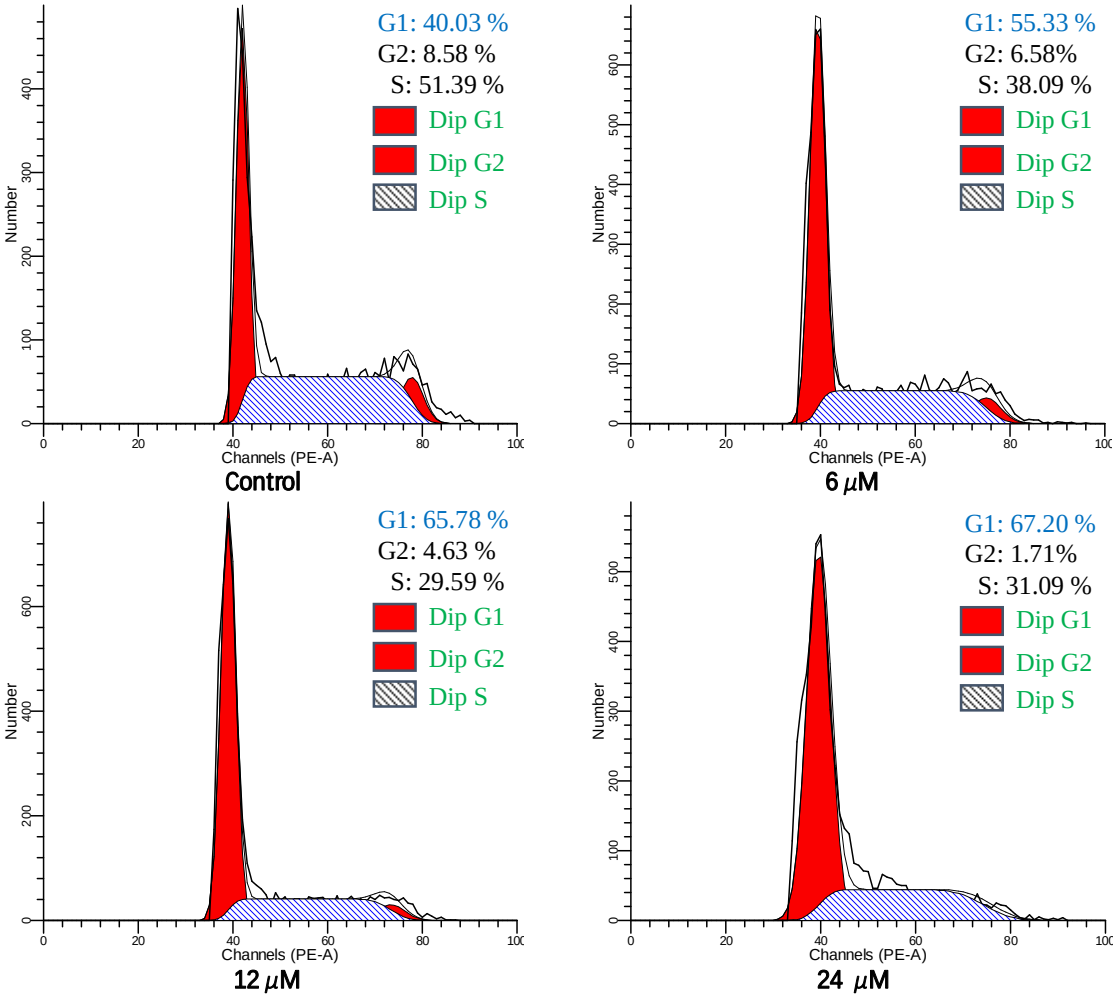

Figure 3. Arrest effects of compound **4** on HeLa cell cycle. HeLa cells were treated with different concentrations (6, 12, and 24 μM) of compound **4** for 48 h. Then, the cells were harvested and stained with propidium iodide (PI), and the cell cycle distribution was analyzed using flow cytometry.

Intracellular ROS increase is one of the crucial factors leading to cell apoptosis.[49,50] To investigate whether compound **4** can promote the production of ROS, the amount of ROS in HeLa cells was measured after exposure to various concentrations of **4**. As the concentrations of **4** increased, there was a significant increase in the ROS levels as shown in the Figure 4. The results indicated that compound **4** may induce apoptosis by increasing the levels of ROS in the cells.

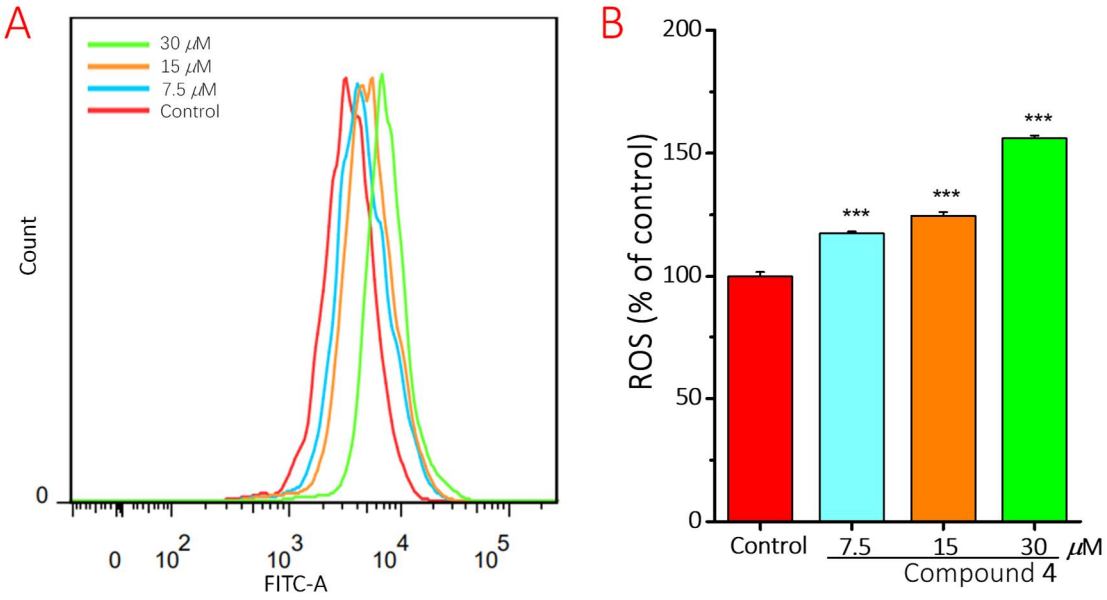

Figure 4. Effects of compound **4** on ROS generation. HeLa cells were treated with compound **4** at the tested concentrations for 48 h. (A) The ROS accumulation in HeLa cells measured by flow cytometer using DCFH-DA staining. (B) Relative ROS levels of HeLa cells after treatment with compound **4** for 48 h. (***) $p < 0.001$ versus control group.

Emerging evidence has demonstrated that activated STAT3 is often observed in tumor cells and acts as a crucial oncogenic mediator and promotes tumorigenesis, tumor immunosuppression, angiogenesis and metastasis.[51,52] Therefore, inhibition of STAT3 or its activation (phosphorylated STAT3, p-STAT3) at tyrosine 705 (Tyr705) provides a potential target for the treatment of various cancers.[52,53] To investigate whether compound **4** can suppress the expression of STAT3 or p-STAT3, western blotting analysis was performed. The present results indicated that compound **4** reduced the protein levels of phosphorylated STAT3, but had no effect on the protein levels of total STAT3 in HeLa cells (Figure 5). In addition, compound **4** inhibited the activation of STAT3 in a dose-dependent manner (Figure 5).

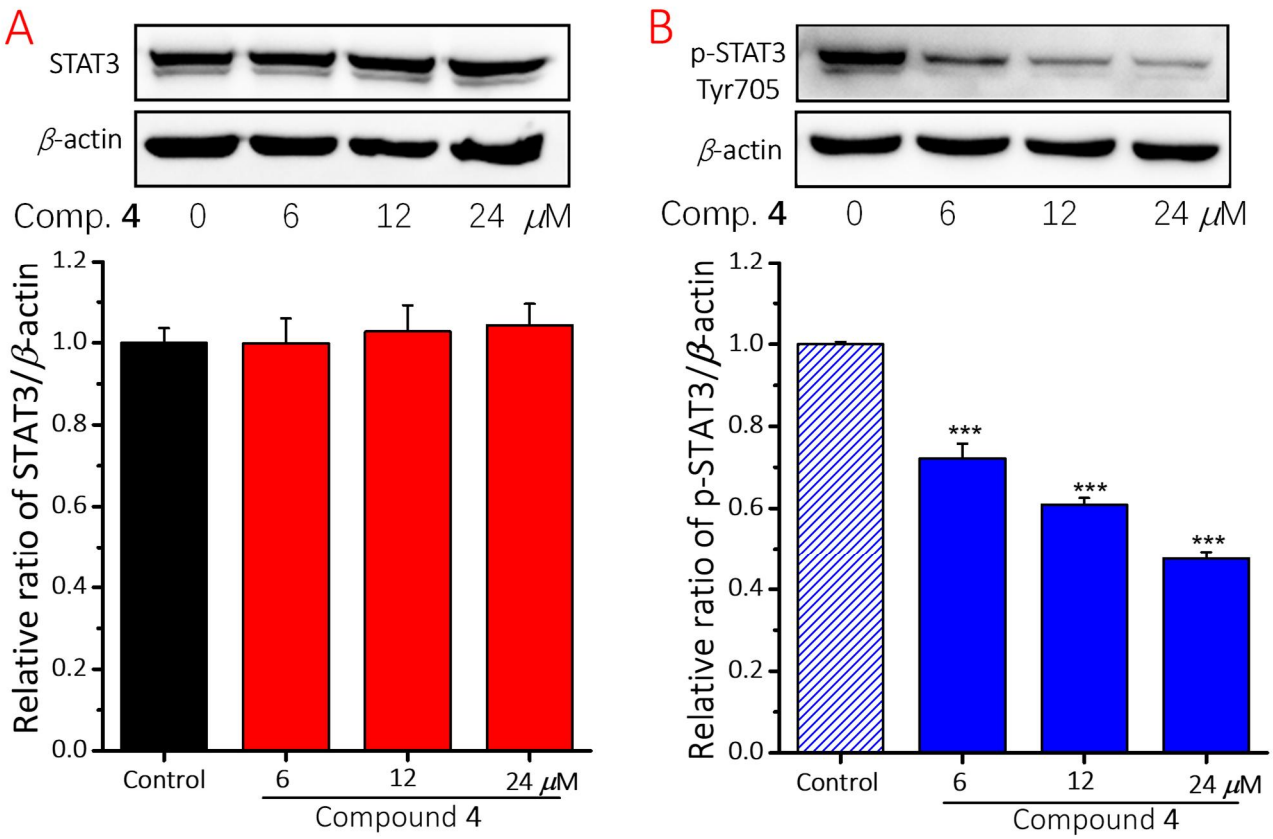

Figure 5. Effects of compound **4** on protein levels of STAT3 and p-STAT3. HeLa cells were treated with compound **4** at the tested concentrations for 12 h and then the cell lysates were harvested and analyzed using the corresponding antibodies by Western blotting analysis. The effects of compound **4** on STAT3 protein levels and the quantitative analysis in HeLa cells by western blotting analysis. (B) The effects of compound **4** on p-STAT3 protein levels and the quantitative analysis in HeLa cells by western blotting analysis. (***) $p < 0.001$ versus control group.

All of the cellular results revealed that compound **4** showed promising cytotoxic activities by blocking the cell cycle, increasing ROS levels, and inhibiting p-STAT3 to induce cell apoptosis. To investigate its in vivo antitumor effects, a zebrafish (*Danio rerio*) tumor xenograft was established by microinjection.[48] As shown in Figure 6, after treated with different concentrations of compound **4**, the intensity and foci of red fluorescence were significantly decreased in a dose-dependent manner, indicating that **4** blocked effectively tumor invasion and metastasis.

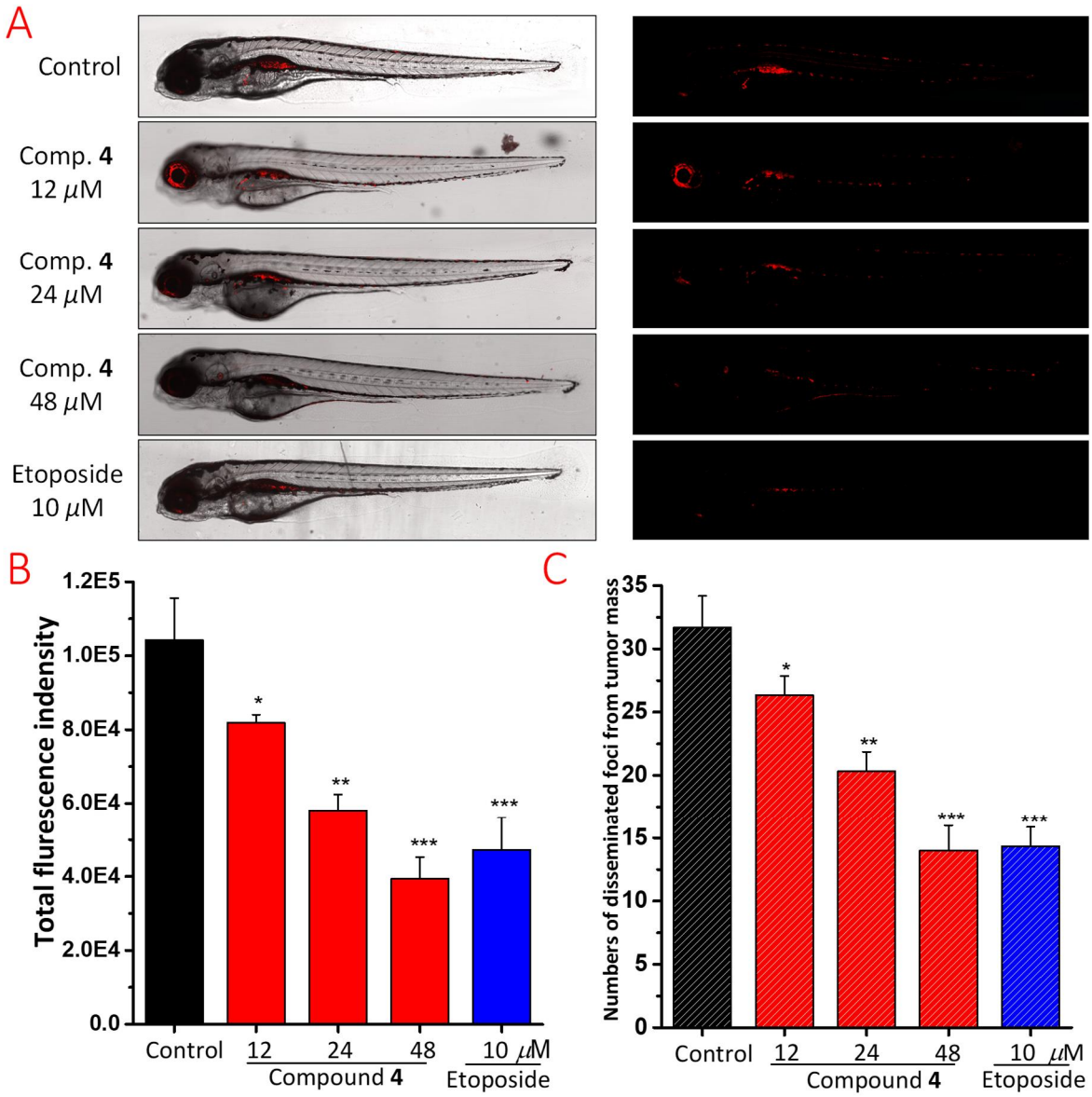

Figure 6. In vivo antitumor effects of compound **4** in zebrafish xenograft. CM-Dil stained HeLa cells were transplanted into 2 dpf zebrafish embryos by microinjecting. Then, 4 h later, tumor-bearing embryos were treated with compound **4** (12, 24, and 48 μM) and etoposide (10 μM) for 48 h (n = 15/group). Intensity and distribution of the red fluorescence were imaged under a confocal microscope (A). Tumor proliferation (B) and metastasis (C) were quantified by Image J. Results were expressed as means ± SD. (*) $p < 0.05$, (**) $p < 0.01$, and (***) $p < 0.001$ versus control group.

The proliferation and metastasis of tumors are closely related to tumor angiogenesis, and the subsequent inhibition of tumor angiogenesis has become a primary target for the development of antitumor drugs.[54,55] To detect inhibitory effects on angiogenesis, a transgenic zebrafish *Tg* (*fli1: EGFP*) with EGFP-labeled endothelial cells was used. After the zebrafish embryos were exposed to different concentrations of **4** for 48 h, the development of intersegmental vessels (ISVs) were photographed (Figure 7) and the total lengths of ISVs were measured and quantified with the use of Image J software

(NIH, Bethesda, MD, USA). After statistical analysis, the average length of ISVs of the control group was found to be 3233.3 μm, and the length decreased in a dose-dependent manner (2476.5 ± 185.8 μm at 12 μM, 2263.2 ± 134.5 μm at 24 μM, and 1881.6 ± 78.0 μm at 48 μM) with the increasing of concentrations of compound **4**.

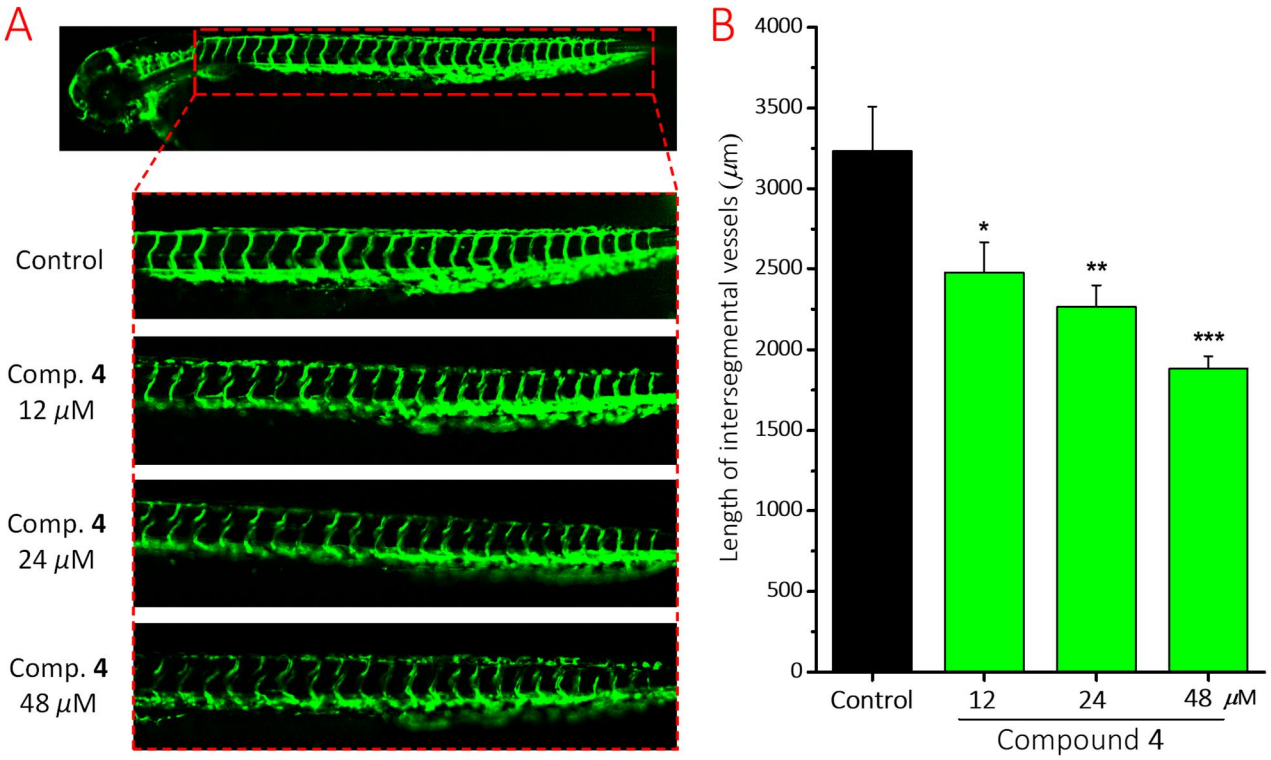

Figure 7. Antiangiogenesis activity of compound **4** in a transgenic zebrafish model. The embryos from transgenic zebrafish *Tg*(*fli1: EGFP*) were treated by compound **4**. After exposure to the compounds for 48 h, the development of intersegmental vessels (ISVs) was observed, and the length of ISV vessels was measured using Image J programme. (A) Representative images of zebrafish embryos treated with vehicle and various concentrations of compound **4**. (B) The average total length of ISVs of zebrafish after treating with different concentrations of compound **4** (12, 24, and 48 μM). (n = 15 for each experimental group). (*) $p < 0.5$, (**) $p < 0.01$, (***) $p < 0.001$ versus control group.

■ EXPERIMENTAL SECTION

General Experimental Procedures. The instruments and materials for compound isolation, identification, and biological evaluation were the same as reported in our previous reports.[47,48]

Plant Material. The leaves of *G. xipshuanbannaensis* were collected from Xishuangbanna, Yunnan Province, People's Republic of China, in April 2018 and identified by one of the authors (Y. G.). A voucher specimen (No. 20180803) has been stored at the laboratory of Natural Medicinal Chemistry, Nankai University.

Extraction and Isolation. The detailed information on extraction and isolation of the leaves of *G. xipshuanbannaensis* is provided in the Supporting Information.

*Xipsxanthone A (**1**):* yellow powder; UV (MeOH) λ_{max} (log ε) 207 (4.01), 247 (4.09), 264 (4.12), 323 (4.21) nm; IR (film) ν_{max} 3405, 2957, 2923, 2859, 1620, 1445, 1377, 1281, 1179 cm^{-1}; ^{1}H NMR (400 MHz, $CDCl_3$) and ^{13}C NMR (100 MHz, $CDCl_3$) data, see Tables 1 and 2; ESIMS *m/z* 531 $[M - H]^-$; HRESIMS *m/z* 531.2753 $[M - H]^-$, calcd for $C_{33}H_{39}O_6$, 531.2747.

*Xipsxanthone B (**2**):* yellow gum; UV (MeOH) λ_{max} (log ε) 208 (4.02), 262 (4.12), 321 (4.20) nm; IR (film) ν_{max} 3351, 2959, 2923, 2859, 1633, 1584, 1443, 1285, 1176 cm^{-1}; ^{1}H NMR (400 MHz, $CDCl_3$) and ^{13}C NMR (100 MHz, $CDCl_3$) data, see Tables 1 and 2; ESIMS *m/z* 549 $[M - H]^-$; HRESIMS *m/z* 549.2855 $[M - H]^-$, calcd for $C_{33}H_{41}O_7$, 549.2852.

*Xipsxanthone C (**3**):* yellow gum; UV (MeOH) λ_{max} (log ε) 206 (4.01), 296 (4.17), 338 (4.23) nm; IR (film) ν_{max} 3424, 2970, 2919, 2860, 1643, 1614, 1474, 1280, 1197, 1164 cm^{-1}; ^{1}H NMR (400 MHz, $CDCl_3$) and ^{13}C NMR (100 MHz, $CDCl_3$) data, see Tables 1 and 2; ESIMS *m/z* 463 $[M - H]^-$; HRESIMS *m/z* 463.2122 $[M - H]^-$, calcd for $C_{28}H_{31}O_6$, 463.2122.

*Xipsxanthone D (**4**):* yellow solid; UV (MeOH) λ_{max} (log ε) 207 (4.01), 244 (4.09), 317 (4.20) nm; IR (film) ν_{max} 3452, 2967, 2925, 2857, 1607, 1461, 1291, 1162, 1120 cm^{-1}; ^{1}H NMR (400 MHz, $CDCl_3$) and ^{13}C NMR (100 MHz, $CDCl_3$) data, see Tables 1 and 2; ESIMS *m/z* 495 $[M + H]^-$; HRESIMS *m/z* 495.2384 $[M + H]^+$, calcd for $C_{29}H_{35}O_7$, 495.2383.

Cytotoxicity Assay, Cell Apoptosis Analysis, Cell Cycle Analysis, ROS Detection, and Western Blotting Analysis. All of the experimental procedures on cell experiments are provided in the Supporting Information.

In vivo Antitumor Assay Using Zebrafish Tumor Xenografts. After breeding by adult AB zebrafish (*Danio rerio*), suitable embryos at 48 h post-fertilization (hpf) were selected and utilized to establish a zebrafish tumor xenograft model according to a previous report.[48] In brief, HepG2 cells first were stained with CM-Dil at a final concentration of 2 μM, and were suspended in FBS-free medium to a density of 1×10^7 cells/mL. Then, 5 *n*L of the stained cells were microinjected into the

yolk sac of anesthetized zebrafish embryos and the embryos were further incubated at 28.5 ℃ for 4 h to establish the zebrafish tumor xenograft model. Subsequently, tumor-bearing embryos were randomly divided into groups (15 embryos/group) and treated with different concentrations of the tested compounds at 28.5 ℃ for 48 h. Etoposide was used as a positive control. At 5 days post-fertilization (dpf), tumor proliferation and migration in the zebrafish embryos were examined by confocal microscopy (Leica, Germany) and analyzed using Image J software (NIH, Bethesda, MD, USA). The density and focus number of red fluorescence representing the proliferation and migration of HepG2 cells in vivo, were statistically analyzed, respectively. All the procedures involving animals were approved by the Institutional Animal Care Committee of Nankai University (No. SYXK (JIN) 2019-0001).

Antiangiogenesis Assay Using Transgenic Zebrafish. An antiangiogenesis activity was detected using transgenic zebrafish *Tg*(*fli1:EGFP*) embryos with EGFP-labelled endothelial cells, according to a method reported previously.[56] After breeding, 6 hpf embryos were exposed to different concentrations of the test compounds and incubated at 28.5 ℃ for 48 h. Then, the embryos were anesthetized with 0.02% tricaine and the development of intersegmental blood vessels (ISVs) were photographed using confocal microscopy (Leica, Germany). The total average length of ISV vessels was measured and quantified using ImageJ software (NIH, Bethesda, MD, USA).

■ ASSOCIATED CONTENT

● Supporting Information

The Supporting Information is available free of charge on the ACS Publications website at DOI:

The NMR spectra of compounds **1**–**4**.

■ AUTHOR INFORMATION

Corresponding Authors

*Tel/Fax (J. Xu): 86-22-23506290. E-mail: xujing611@nankai.edu.cn.

*Tel/Fax (Y. Guo): 86-22-23507760. E-mail: victgyq@nankai.edu.cn.

ORCID

Jing Xu: 0000-0003-0847-4510

Yuanqiang Guo: 0000-0002-5297-0223

Author Contributions

¶X. Zhang and Z. Song contributed equally to this work.

Notes

The authors declare no competing financial interest.

■ ACKNOWLEDGMENTS

This research was supported financially by the National Natural Science Foundation of China (Nos. 22077067, U1801288, and 21665013), and the Natural Science Foundation of Tianjin, China (No. 19JCYBJC28100).

REFERENCES

(1) Hemshekhar, M.; Sunitha, K.; Santhosh, M. S.; Devaraja, S.; Kemparaju, K.; Vishwanath, B. S.; Girish, K. S. *Phytochem. Rev.* **2011**, *10*, 325–351.

(2) Espirito Santo, B. L. S. D., Santana, L. F., Kato Junior, W. H., de Araújo, F. D. O., Bogo, D., Freitas, K. D. C., Guimarães, R. C. A.; Hiane, P. A.; Pott, A.; Filiú, W. F. O.; Arakaki Asato, M.; Figueiredo, P. O.; Bastos, P. R. H. O. *Molecules* **2020**, *25*, 4513.

(3) Zhang, S.; Li, Z.; Wang, X.; An, L.; Bao, J.; Zhang, J.; Cui, J.; Li, Y.; Jin, D. Q.; Tuerhong, M. *Carbohyd. Polym.* **2020**, *246*, 116567.

(4) Zhang, S.; An, L.; Li, Z.; Wang, H.; Shi, L.; Zhang, J.; Li, Y.; Jin, D. Q.; Tuerhong, M.; Ohizumi, Y. *Carbohyd. Polym.* **2020**, *235*, 115929.

(5) Liu, X. J.; Hu, X.; Peng, X. H.; Wang, Y. T.; Huang, X. F.; Zan, Y. H.; Li, D. H.; Li, Z. L.; Hua, H. M. *Bioorg. Chem.* **2020**, *94*, 103370.

(6) Wang, Y. L.; Ye, Y. S.; Fu, W. W.; Wu, R.; Xiang, Q.; Lao, Y. Z.; Yang, J. L.; Tan, H. S.; Yang, X. W.; Yang, B. C. *Org. Let.* **2019**, *21*, 1534–1537.

(7) Niu, S. L.; Li, D. H.; Li, X. Y.; Wang, Y. T.; Li, S. G.; Bai, J.; Pei, Y. H.; Jing, Y. K.; Li, Z. L.; Hua, H. M. *J. Nat. Prod.* **2018**, *81*, 749–757.

(8) Jia, C. C.; Xue, J. J.; Gong, C.; Li, X. Y.; Li, D. H.; Li, Z. L.; Hua, H. M. *Fitoterapia* **2018**, *127*, 220–225.

(9) Niu, S. L.; Li, D. H.; Wang, Y. T.; Wang, K. B.; Lin, B.; Jing, Y. K.; Hua, H. M.; Bai, J.; Li, Z. L. *Org. Biomol. Chem.* **2017**, *15*, 4901–4906.

(10) Wang, J.; Wang, L.; Ho, C. T.; Zhang, K.; Liu, Q.; Zhao, H. *J. Agric. Food Chem.* **2017**, *65*, 3675–3683.

(11) Gao, X. M.; Ji, B. K.; Li, Y. K.; Ye, Y. Q.; Jiang, Z. Y.; Yang, H. Y.; Hu, Q. F. *Chem. Soc.* **2016**, *27*, 10–14.

(12) Hu, Q.; Ning, P.; Li, L.; Lou, J.; Cheng, Y.; Shi, L.; Shu, D.; Gao, X. M.; Yang, Y.; Wang, Y. *Heterocycles* **2015**, *91*, 375–380.

(13) Li, D. H.; Li, C. X.; Jia, C. C.; Sun, Y. T.; Xue, C. M.; Bai, J.; Hua, H. M.; Liu, X. Q.; Li, Z. L. *Arch. Pharm. Res.* **2016**, *39*, 172–177.

(14) Li, Y.; Wang, Z.; Wu, X.; Yang, Y.; Qin, Y.; Xia, C.; Meng, Y.; Li, M.; Gao, X. M.; Hu, Q. *Phytochem. Lett.* **2015**, *11*, 24–27.

(15) Feng, C.; Huang, S. X.; Gao, X. M.; Xu, H. X.; Luo, K. Q. *J. Nat. Prod.* **2014**, *77*, 1111–1116.

(16) Shen, T.; Li, W.; Wang, Y. Y.; Zhong, Q. Q.; Wang, S. Q.; Wang, X. N.; Ren, D. M.; Lou, H. X. *Arch. Pharm. Res.* **2014**, *37*, 412–420.

(17) Niu, S. L.; Li, Z. L.; Ji, F.; Liu, G. Y.; Zhao, N.; Liu, X. Q.; Jing, Y. K.; Hua, H. M. *Phytochemistry* **2012**, *77*, 280–286.

(18) Gao, X. M.; Yu, T.; Cui, M. Z.; Pu, J. X.; Du, X.; Han, Q. B.; Hu, Q. F.; Liu, T. C.; Luo, K. Q.; Xu, H. X. *Bioorg. Med. Chem. Let.* **2012**, *22*, 2350–2353.

(19) Ren, Y.; Yuan, C.; Chai, H. B.; Ding, Y.; Li, X. C.; Ferreira, D.; Kinghorn, A. D. *J. Nat. Prod.* **2011**, *74*, 460–463.

(20) Lee, P. S.; Teng, C. Y.; Kalyanam, N.; Ho, C. T.; Pan, M. H. *Mol. Nutr. Food Res.* **2019**, *63*, 1800390.

(21) Wang, Y.; Tsai, M. L.; Chiou, L. Y.; Ho, C. T.; Pan, M. H. *J. Agric. Food Chem.* **2015**, *63*, 9047–9052.

(22) Hung, W. L.; Liu, C. M.; Lai, C. S.; Ho, C. T.; Pan, M. H. *J. Funct. Foods* **2015**, *18*, 432–444.

(23) Hung, W. L.; Tsai, M. L.; Sun, P. P.; Tsai, C. Y.; Yang, C. C.; Ho, C. T.; Pan, M. H. *Food Funct.* **2014**, *5*, 2883–2891.

(24) Tsai, M. L.; Chiou, Y. S.; Chiou, L. Y.; Ho, C. T.; Pan, M. H. *Mol. Nutr. Food Res.* **2014**, *58*, 1820–1829.

(25) Editorial Committee of the Flora of China, Chinese Academy of Sciences. *Flora of China*; Vol. *50* (2); Science Press: Beijing, 1990; p 98.

(26) Han, Q. B.; Yang, N. Y.; Tian, H. L.; Qiao, C. F.; Song, J. Z.; Chang, D. C.; Chen, S. L.; Luo, K. Q.; Xu, H. X. *Phytochemistry* **2008**, *69*, 2187–2192.

(27) Zhou, Y.; Han, Q. B.; Song, J. Z.; Qiao, C. F.; Xu, H. X. *J. Chromatogr. A* **2008**, *1206*, 131–139.

(28) Na, Z.; Xu, Y. K. *Nat. Prod. Res.* **2010**, *24*, 1648–1653.

(29) Jo, Y. H.; Kim, S. B.; Ahn, J. H.; Turk, A.; Kwon, E. B.; Kim, M. O.; Lee, M. K. *Bioorg. Chem.* **2019**, *92*, 103234.

(30) Xue, Q.; Chen, Y.; Yin, H.; Teng, H.; Qin, R.; Liu, H.; Li, Q.; Mei, Z.; Yang, G. *Bioorg. Chem.* **2020**, *104*, 104339.

(31) Gao, X. M.; Yu, T.; Lai, F. S. F.; Zhou, Y.; Liu, X.; Qiao, C. F.; Song, J. Z.; Chen, S. L.; Luo, K. Q.; Xu, H. X. *Bioorg. Med. Chem.* **2010**, *18*, 4957–4964.

(32) Teng, H.; Ma, Z.; Teng, H.; Du, Y.; Chen, X.; Chen, Y.; Yang, G. *Nat. Prod. Res.* **2020**, 1–7.

(33) Yang, J.; Fu, W.; Xiang, Q.; Tang, Y.; Wu, R.; Zheng, C.; Lu, Y.; Zhou, H.; Xu, H. *Phytochemistry* **2020**, *174*, 112329.

(34) Tang, Y. X.; Fu, W. W.; Wu, R.; Tan, H. S.; Shen, Z. W.; Xu, H. X. *J. Nat. Prod.* **2016**, *79*, 1752–1761.

(35) Han, A. R.; Kim, J. A.; Lantvit, D. D.; Kardono, L. B. S.; Riswan, S.; Chai, H.; Carcache de Blanco, E. J.; Farnsworth, N. R.; Swanson, S. M.; Kinghorn, A. D. *J. Nat. Prod.* **2009**, *72*, 2028–2031.

(36) Zou, Y. S.; Hou, A. J.; Zhu, G. F.; Chen, Y. F.; Sun, H. D.; Zhao, Q. S. *Bioorg. Med. Chem.* **2004**, *12*, 1947–1953.

(37) Ha, L. D.; Hansen, P. E.; Vang, O.; Duus, F.; Pham, H. D.; Nguyen, L. H. D. *Chem. Pharm. Bull.* **2009**, *57*, 830–

834.

(38) Sen, A. K.; Sarkar, K. K.; Mazumder, P. C.; Banerji, N.; Uusuori, R.; Hase, T. A. *Phytochemistry* **1982**, *21*, 1747–1750.

(39) Azebaze, A. G. B.; Meyer, M.; Valentin, A.; Nguemfo, E. L.; Fomum, Z. T.; Nkengfack, A. E. *Chem. Pharm. Bull.* **2006**, *54*, 111–113.

(40) Bennett, G. J.; Harrison, L. J.; Sia, G. L.; Sim, K. Y. *Phytochemistry* **1993**, *32*, 1245–1251.

(41) Nagem, T. J.; Werle, A. A.; Carvalho, M. G. D.; Mesquita, A. A. L. *J. Braz. Chem. Soc.* **1997**, *8*, 285–288.

(42) Shen, J.; Yang, J. S. *Chem. Pharm. Bull.* **2006**, *54*, 126–128.

(43) Ren, Y.; Carcache de Blanco, E. J.; Fuchs, J. R.; Soejarto, D. D.; Burdette, J. E.; Swanson, S. M.; Kinghorn, A. D. *J. Nat. Prod.* **2019**, *82*, 657–679.

(44) Ren, Y.; Matthew, S.; Lantvit, D. D.; Ninh, T. N.; Chai, H.; Fuchs, J. R.; Soejarto, D. D.; Carcache de Blanco, E. J.; Swanson, S. M.; Kinghorn, A. D. *J. Nat. Prod.* **2011**, *74*, 1117–1125.

(45) Gong, G.; Chen, H.; Kam, H.; Chan, G.; Tang, Y. X.; Wu, M.; Tan, H.; Tse, Y. C.; Xu, H. X.; Lee, S. M. Y. *J. Nat. Prod.* **2020**.

(46) Kwon, J.; Hiep, N. T.; Kim, D. W.; Hong, S.; Guo, Y.; Hwang, B. Y.; Lee, H. J.; Mar, W.; Lee, D. *J. Nat. Prod.* **2016**, *79*, 1938–1951.

(47) Liu, F.; Ma, J.; Shi, Z.; Zhang, Q.; Wang, H.; Li, D.; Song, Z.; Wang, C.; Jin, J.; Xu, J.; Tuerhong, M.; Abudukeremu, M.; Shuai, L.; Lee, D.; Guo, Y. *J. Nat. Prod.* **2020**, *83*, 36–44.

(48) Liang, Y.; Zhang, Q.; Yang, X.; Li, Y.; Zhang, X.; Li, Y.; Du, Q.; Jin, D. Q.; Cui, J.; Lall, N.; Tuerhong, M.; Lee, D.; Abudukeremu, M.; Xu, J.; Shuai, L.; Guo, Y. *Bioorg. Chem.* **2020**, 103741.

(49) Ye, Y.; Zhang, T.; Yuan, H.; Li, D.; Lou, H.; Fan, P. *J. Med. Chem.* **2017**, *60*, 6353–6363.

(50) Lin, Z.; Guo, Y.; Gao, Y.; Wang, S.; Wang, X.; Xie, Z.; Niu, H.; Chang, W.; Liu, L.; Yuan, H.; Lou, H. *J. Med. Chem.* **2015**, 58, 3944–3956.

(51) Yu, H.; Lee, H.; Herrmann, A.; Buettner, R.; Jove, R. *Nat. Rev. Cancer* **2014**, *14*, 736–746.

(52) Furtek, S. L.; Backos, D. S.; Matheson, C. J.; Reigan. P. *ACS Chem. Biol.* **2016**, *11*. 308–318.

(53) Laudisi, F.; Cherubini, F.; Monteleone, G.; Stolfi. C. *Int. J. Mol. Sci.* **2018**, *19*, 1787.

(54) Lugano, R.; Ramachandran, M.; Dimberg, A. *Cell. Mol. Life Sci.* **2020**, *77*, 1745–1770.

(55) Kerbel, R. S. *N. Engl. J. Med.* **2008**, *358*, 2039–2049.

(56) Jiang, X.; Zhou, J.; Lin, Q.; Gong, G.; Sun, H.; Liu, W.; Guo, Q.; Feng, F.; Qu, W. *Bioorg. Med. Chem.* **2018**, *26*, 4481–4492.

Table of Contents/Abstract Graphic